ANALYSIS OF THE PERFORMANCE OF DIFFERENT SEDIMENT TRANSPORT FORMULATIONS IN NON-HYDROSTATIC XBEACH

Giulia Mancini[1], Riccardo Briganti[2], Gioele Ruffini[3], Robert McCall[4], Nicholas Dodd[5], Fangfang Zhu [6]

Process-based, wave-resolving models are essential tools to resolve the complex hydro-morphodynamics in the swash zone. The open-source Non-Hydrostatic XBeach model can solve the depth-averaged wave-by-wave flow in the nearshore region up to the shoreline and the intra-wave bed changes during time-varying storms. However, validation and testing of its morphological response are still limited in the context of sandy beaches. This work aims to assess the performance of the wave-resolving sediment dynamics modelling within Non-Hydrostatic XBeach for different sediment transport formulations. The sediment transport modelling approaches considered in this study were tested and compared to laboratory experiments involving wave trains over an intermediate beach. Numerical results show a better performance in the prediction of the intra-swash sediment dynamics when the newly implemented wave-resolving transport equation is applied compared to the existing approach within the model.

Keywords: wave-resolving modelling; sediment transport; beach morphodynamics; swash zone; surf zone

INTRODUCTION

Process-based, wave-resolving models are essential tools to resolve the complex hydro-morphodynamics in the swash zone. They include intra-wave physical processes, which are necessary to describe the sediment dynamics in this zone when swash-swash interactions are present. These interactions can influence the seaward directed sediment transport, which feeds the development of a beach profile (e.g., the migration of bars, Alsina et al., 2012). Currently, few existing models are able to resolve the intra-swash hydro-morphodynamics. Wave-resolving models are of two types: depth-averaged and depth-resolving models. The latter type of models can simulate the vertical structure of the flow in the surf and swash zones. However, their validation, at present, is limited to relatively simple wave and morphodynamics conditions, such as sediment transport induced by isolated waves (e.g., Li et al., 2019), or to a limited area only when laboratory experiments are simulated (e.g., Jacobsen et al., 2014; Kim et al., 2019; Larsen et al., 2020). The present study uses a depth-averaged, wave-resolving framework because this approach is the most practically used for engineering practice. The lack of a full description of the velocity profile makes this type of models less computationally demanding. The governing hydrodynamics equations of depth-averaged, wave-resolving models are the Non Linear Shallow Water Equations (NLSWE) (e.g., Postacchini et al., 2012; Zhu and Dodd, 2015; Incelli et al., 2016, see Briganti et al., 2016 for a review), the non-hydrostatic NLSWE (e.g., Smit et al., 2010; Ma et al., 2012; Ruffini et al., 2020), or the Boussinesq-type equations (e.g., Xiao et al., 2010; Kim et al., 2017). The former set of flow equations do not take into account the wave dispersion, thus limiting their application when compared to the latter two types of equations. The non-hydrostatic NLSWE and the Boussinesq-type equations are widely used to simulate the wave propagation from intermediate waters to the shoreline. The morphodynamics in these models is computed by combining the aforementioned hydrodynamics equations with a sediment conservation equation and a bed-updating equation. The open-source Non-Hydrostatic XBeach (XBNH) model (Smit et al., 2010) can solve the depth-averaged wave-by-wave flow in the nearshore region up to the shoreline and in turn, intra-wave bed changes during varying time scales. Formulations of sediment transport within XBNH have been extensively tested for gravel beaches (e.g., McCall et al., 2015). However, validation and testing of XBNH morphological response in the context of sandy beaches are still limited. The existing approach in the model has been originally formulated for the wave-averaged version of XBeach. Therefore, there is no knowledge of which is the best sediment transport approach to use within XBNH.

The aim of this study is to assess the performance of the wave-resolving sediment dynamics modelling within XBNH for different sediment transport formulations. Two main objectives are pursued. First, an Intra-Wave Sediment Transport formulation is newly implemented in XBNH (XBNH-IWST). In particular, the Pritchard and Hogg (2003) transport equation for the suspended sediment concentration is included in

[1]Department of Civil Engineering, University of Nottingham, Nottingham, NG7 2RD, UK
[2]Department of Civil Engineering, University of Nottingham, Nottingham, NG7 2RD, UK
[3]Department of Civil Engineering, University of Nottingham, Nottingham, NG7 2RD, UK
[4]Department of Applied Morphodynamics, Deltares, Delft, 2629 HV, The Netherlands
[5]Department of Civil Engineering, University of Nottingham, Nottingham, NG7 2RD, UK
[6]Department of Civil Engineering, University of Nottingham Ningbo China, Ningbo, 315100, China

XBNH and the Meyer-Peter and Müller (1948) expression is considered for the bed load transport. These two formulations are chosen because of their good performance in the swash zone (see Zhu and Dodd, 2015). In Mancini et al. (2020), which mainly focuses on the swash zone, the combined use of the Pritchard and Hogg (2003) and the Meyer-Peter and Müller (1948) formula within XBNH are verified against the semi-analytical solution of Zhu and Dodd (2015). Instead, in the present work, the performance of these formulations and a comparison of their response with the existing approach originally developed for the Wave-Averaged Sediment Transport model within XBNH (XBNH-WAST) are analysed for the swash and the surf zones. The model response is tested against laboratory experiments where swash-swash interactions were present.

The paper is organized as follows: in the first section XBNH-WAST and XBNH-IWST are described; the performance of the two approaches against laboratory experiments are presented in the second section; discussion of results and concluding remarks with recommendations for future works are given in the third and in the forth section, respectively.

NUMERICAL MODEL DESCRIPTION

XBNH consists of coupled wave-resolving hydrodynamics and morphodynamics equations. In this study the existing XBNH-WAST approach uses the Van Rijn (2007) and Van Thiel de Vries (2008) formulations, which were originally developed for the wave-averaged version of the model. Whereas, the newly implemented XBNH-IWST approach considers two wave-resolving sediment transport formulations (i.e., the Pritchard and Hogg, 2003 and Meyer-Peter and Müller, 1948 expressions). In this work only the cross-shore direction is considered.

Hydrodynamics equations

The hydrodynamics in XBNH is similar to the one-layer version of the SWASH model (Zijlema et al., 2011). The depth-averaged flow is computed using the non-hydrostatic 1D (one-dimensional) NLSWE with the continuity and momentum equations given by:

$$\frac{\partial \eta}{\partial t} + \frac{\partial hu}{\partial x} = 0, \tag{1}$$

$$\frac{\partial u}{\partial t} + u\frac{\partial u}{\partial x} - \frac{\partial}{\partial x}\left(\nu_h \frac{\partial u}{\partial x}\right) = -\frac{1}{\rho}\frac{\partial(\rho p_{nh} + \rho g\eta)}{\partial x} - \frac{\tau_b}{\rho h}, \tag{2}$$

where t is time, η is the water surface elevation, u is the depth-averaged cross-shore velocity, h is the total water depth, ν_h is the horizontal viscosity computed using the Smagorinsky (1963) model, ρ is the density of water, p_{nh} is the depth-averaged dynamic pressure normalized by the density, g is the gravity acceleration constant and τ_b is the total bed shear stress, which is computed as:

$$\tau_b = \rho c_f u|u|, \tag{3}$$

where c_f is the dimensionless friction coefficient. In the cases analysed in this study the dispersivity parameter, $k_w d$, is lower than 0.5, where k_w is the wave number (defined as $k_w = 2\pi/L$, with L being the local wave length) and d is the still water depth. Therefore, the celerity error in the description of frequency dispersion is of the order of 1% (Bai et al., 2018).

Wave breaking in XBNH is modelled by using the Hydrostatic Front Approximation (HFA) of Smit et al. (2013), in which the non-hydrostatic pressure term is set to zero when a maximum wave steepness is reached, and waves propagate as hydrostatic bores. The reader is referred to Smit et al. (2010) for a full description of the XBNH model.

Sediment transport equations in XBNH-WAST

In XBNH-WAST the equation for the sediment transport is formulated as:

$$\frac{\partial hC}{\partial t} + \frac{\partial\left[\left(huC + D_C h\frac{\partial C}{\partial x}\right)S_{sl}\right]}{\partial x} = \frac{hC_{eq} - hC}{w_s} = E - D, \tag{4}$$

where C is the depth-averaged suspended sediment concentration and C_{eq} is the total sediment equilibrium concentration and D_C is the diffusion coefficient (Deltares, 2015). The maximal value of C, C_{max}, is herein

considered as the higher physically possible sediment concentration for a fluidised bed and defined as: $C_{max} = 1 - n_{p,d}$, with $n_{p,d} = 0.6$, the porosity for a fluidized bed; S_{sl} represents the bed slope effects computed following Deltares (2015):

$$S_{sl} = 1 - \alpha_{sl}\frac{\partial z_b}{\partial x}, \tag{5}$$

where $\alpha_{sl} = 0.15$ according to Deltares (2015) and z_b is the bed level. Therefore, the sediment transport rate, q_s, is computed as $q_s = (huC + D_C h\partial C/\partial x)S_{sl}$; w_s is the sediment settling velocity. The two terms on the right side represent the erosion rate, E, and the deposition rate, D. When $E = D$, nor erosion or deposition occurs; as a consequence, $C_{eq} = C$. The Van Rijn et al. (2007) and Van Thiel de Vries (2008) formulations compute first the equilibrium concentration for bed load and for suspended load separately, and then the total one. For both the bed load and the suspended load, referred to as b and s, respectively, the equilibrium concentrations, $C_{eq,b}$, and $C_{eq,s}$, are expressed in function of u and the root-mean-square wave orbital velocity, u_{rms}, as:

$$C_{eq,b,s} = \frac{A_{b,s}}{h}\left(\sqrt{u^2 + 0.64u_{rms}^2} - u_{cr}\right)^{\gamma_2}, \tag{6}$$

where $A_{b,s}$ represents the bed load and suspended load coefficients, depending on sediments grain size and flow properties, $\gamma_2 = 1.5$ for bed load and $\gamma_2 = 2.4$ for suspended load. u_{cr} is the critical velocity determined as a function ("ϕ") of u and u_{rms}: $u_{cr} = \phi(|u|/(|u| + u_{rms}))$. The bed load transport rate, q_b, is computed as $q_b = uhC_{eq,b}S_{sl}$. The reader is referred to Deltares (2015) for a more detailed description of XBNH-WAST.

Sediment transport equations in XBNH-IWST

In this study, the Pritchard and Hogg (2003) equation for the intra-wave suspended sediment transport is included in XBNH with the addition of a diffusion term similarly to XBNH-WAST:

$$\frac{\partial hC}{\partial t} + \frac{\partial\left[\left(huC + D_C h\frac{\partial C}{\partial x}\right)S_{sl}\right]}{\partial x} = m_e\left(\frac{\tau_b - \tau_{b,cr}}{\tau_{ref}}\right)^R - w_s C_{nb} = E - D, \tag{7}$$

Similarly to XBNH-WAST, q_s, is defined as: $q_s = (huC + D_C h\partial C/\partial x)S_{sl}$. m_e is the mobility parameter, which determines the erodibility of the sediment as suspended load, $\tau_{b,cr}$ is the critical bed shear stress, τ_{ref} is the reference bed shear stress, $R > 0$ is a dimensionless exponent (Pritchard and Hogg, 2003), and C_{nb} is the near-bed suspended sediment concentration at a small near-bed reference height, d_{nb}, above z_b. C_{nb} in D is computed as:

$$C_{nb} = CK_C, \tag{8}$$

where the shape factor, K_C, represents the relative importance of sediment settling and mixing. When good mixing is assumed, $K_C = 1$. K_C depends only on sediment properties and the depth-averaged hydrodynamics. Consequently:

$$K_C = \frac{(1 - B)}{d'_{nb}({d'_{nb}}^{B-1} - 1)}, \tag{9}$$

where B is the Rouse number and d'_{nb} is the dimensionless near-bed reference height, given by a simplified form of Van Rijn formula as shown in Soulsby (1997) with the relationship:

$$d'_{nb} = \frac{d_{nb}}{h} = 0.519\left(\frac{D_{50}}{\lambda}\right)^{0.3}, \tag{10}$$

in which D_{50} is the median grain diameter, and λ is a reference length-scale.

q_b is calculated using the equation derived by Meyer-Peter and Müller (1948):

$$q_b = 8(\theta - \theta_{cr})^{1.5}\sqrt{\Delta g D_{50}^3}\frac{\tau_b}{|\tau_b|}S_{sl}, \tag{11}$$

where θ and θ_{cr} are the Shields and critical Shields parameters, respectively; $\Delta = (\rho_s - \rho)/\rho$, in which ρ_s is the sediment density. θ is computed as $\theta = \tau_b/(\Delta\rho g D_{50})$, and θ_{cr} is given by Soulsby (1997). The Meyer-Peter and Müller (1948) formula is considered appropriate for the swash zone according to previous studies (see e.g., Chardón-Maldonado et al., 2016). Variations of the formula have been tested, for example, in Postacchini et al. (2012) for sand, while O'Donoghue et al. (2016) and Briganti et al. (2018) for coarse sand. When compared to the original Meyer-Peter and Müller (1948) formula the Postacchini et al. (2012) formulation showed very similar results in terms of net bed changes (see Briganti et al., 2016).

The reader is referred to Mancini et al. (2020) for a more detailed description of XBNH-IWST.

Bed-updating equation

For both XBNH-WAST and XBNH-IWST, the bed-updating is modelled using the Exner-type equation:

$$(1-n_p)\frac{\partial z_b}{\partial t} + E - D + \frac{\partial q_b}{\partial x} = 0, \tag{12}$$

where n_p is the bed porosity.

NUMERICAL MODEL RESULTS

The performance of XBNH-WAST and XBNH-IWST is quantified by computing the normalised Root-Mean-Squared Error (nRMSE), defined as:

$$nRMSE = \frac{\sqrt{\frac{1}{N}\Sigma_i^N (y_{m,i} - y_{ref,i})^2}}{s_{y_{ref}}}, \tag{13}$$

where $y_{m,i}$ is the i-th sample of the modelled quantity y, and $y_{ref,i}$ is the i-th sample of the corresponding reference sample (e.g., experimental); N is the number of samples; $s_{y_{ref}}$ is the standard deviation of the reference quantity y_{ref} and it is defined as:

$$s_{y_{ref}} = \sqrt{\frac{1}{N-1}\Sigma_i^N (y_{ref,i} - \bar{y}_{ref})^2}, \tag{14}$$

with $\bar{y}_{ref} = (1/N)\Sigma_i^N y_{ref,i}$ being the mean value of y_{ref}. nRMSE = 0 indicates perfect agreement between model predictions and reference quantities; whereas nRMSE = 1 indicates that the Root-Mean-Square Error (RMSE) equals $s_{y_{ref}}$.

To further assess the correlation between time series of modelled and reference quantities the Pearson's cross-correlation coefficient, -1 $\leq \rho_{mr} \leq$ 1, is used and it is defined as:

$$\rho_{mr} = \frac{cov(y_{ref}, y_m)}{s_{y_{ref}} s_{y_m}}, \tag{15}$$

where $cov(y_{ref}, y_m)$ is the covariance of the time series of modelled and reference quantities and it is computed as:

$$cov(y_{m,i}, y_{ref,i}) = \frac{1}{(N-1)}\Sigma_i^N (y_{m,i} - \bar{y}_m)(y_{ref,i} - \bar{y}_{ref}), \tag{16}$$

where $\bar{y}_m = (1/N)\Sigma_i^N y_{m,i}$ is the mean value of y_m, and s_{y_m} is the standard deviation of the time series of the predicted quantity.

Numerical simulations of bichromatic wave groups on an intermediate beach

The performance of XBNH-WAST and XBNH-IWST is tested and compared against the experiments conducted within the Hydralab IV - CoSSedM (Coupled High Frequency Measurement of Swash Sediment Transport and Morphodynamics) project (see Alsina et al., 2016). The experiments investigated the hydro-morphodynamics of bichromatic wave groups on a 1:15 sloped beach built at prototype scale with commercial sand characterized by D_{50} = 0.25 mm, w_s = 0.034 m/s, and n_p = 0.36, which clearly showed swash-swash interactions. Two bichromatic wave group conditions with the same energy content were generated in the flume: BE1_2 (broad-banded wave condition) and BE4_2 (narrow-banded wave condition), respectively, with varying wave group period, T_g, and repeat period, T_r. For BE1_2 T_g = 15 s and T_r = 195 s; whereas for BE4_2 $T_g = T_r$ = 27.7 s. $T_g = 1/f_g$, where f_g is the group frequency, which is defined as the difference of the primary components frequencies, f_1 and f_2. A summary of the bichromatic wave groups is shown in Table 1, where H_1 and H_2 are the wave heights of the primary components. For each wave condition, starting from the same initial z_b (around 1:15 uniform sloped bed), eight successive bichromatic waves sequences, from SEG1 to SEG8, each of 1800 s duration, were generated. Fig. 1 shows the initial z_b and the locations of the instruments in the wave flume and selected for comparison. Wave gauges (WG) and Acoustic Wave Gauges (AWG) measured η; Acoustic Doppler Velocimeters (ADV) measured the local flow velocity. Optical Back-Scattering sensors (OBS) and Conductivity Concentration Measurements (CCM$^+$) tanks measured C_z and time-dependent z_b in the swash zone, respectively. d in the horizontal part of the

domain was 2.48 m for BE1_2 and 2.46 m for BE4_2. The reader is referred to Alsina et al. (2016) for a detailed description of the experimental procedure.

In this study, only the first two segments, SEG1 and SEG2, were simulated for both BE1_2 and BE4_2, because those segments showed larger morphological changes than the subsequent ones. For BE1_2 the experimental bed evolution reached an equilibrium more rapidly compared to BE4_2. However, SEG1 and SEG2 were far from equilibrium for both cases.

Table 1: Bichromatic wave groups for BE1_2 and BE4_2 wave conditions

	BE1_2	**BE4_2**
T_g (s)	15	27.7
T_r (s)	195	27.7
f_1 (Hz)	0.303	0.288
H_1 (m)	0.30	0.28
f_2 (Hz)	0.237	0.252
H_2 (m)	0.26	0.30
f_g (m)	0.067	0.036

XBNH-WAST set-up and parameters As shown in Fig. 1, the upstream boundary in the model is located at $x_0 = 30.55$ m, where the WG3 was installed. Thus, the model domain extended from WG3 to the end of the beach, located at $x = 85.05$ m, and like the cited study $\Delta x = 0.1$ m. Time series of η and u were updated as offshore forcing at the upstream boundary. The reader is referred to Ruffini et al. (2020) for a detailed description of the procedure used to obtain the optimal boundary conditions. For c_f, a Manning coefficient, $n = 0.02$, was used, which reflects the characteristics of the considered sandy beach. Model parameters, which are not mentioned herein were set to their default values defined in Deltares (2015).

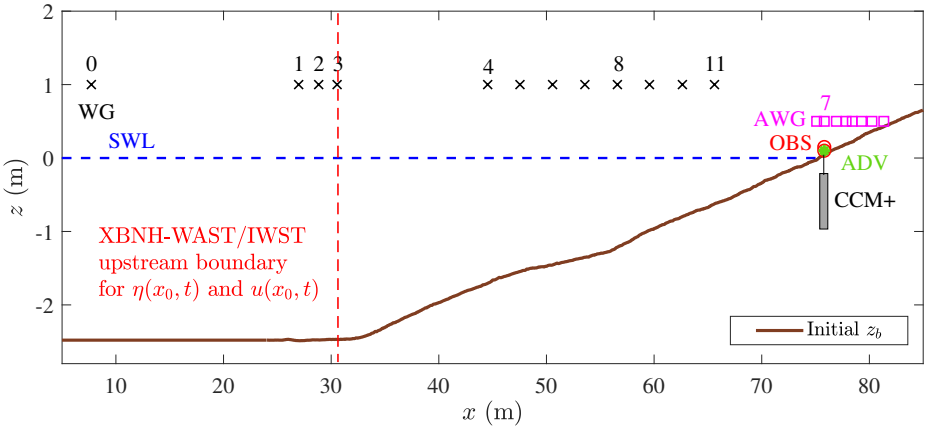

Figure 1: Alsina et al. (2016) experimental domain with main instrumentation installed and upstream boundary condition in XBNH-WAST and XBNH-IWST models domain (red-dashed line); SWL is the Still Water Level

XBNH-IWST set-up and parameters The model domain is the same as in XBNH-WAST as well as the time series of η and u were updated as offshore forcing at the upstream boundary. For the computation of c_f a slightly lower value of the Manning coefficient, n, than in XBNH-WAST was used. $n = 0.018$ s/m$^{1/3}$ was calibrated considering the best compromise between the accuracy of maximum run-up and morphological evolution. Model parameters, which are not mentioned herein were set to their default values defined in Deltares (2015). The calibration of the sediment transport model in XBNH-IWST was carried out by

varying m_e, R, and λ. Table 2 summarizes the main parameters included in the Pritchard and Hogg (2003) transport equation. This set of parameters was chosen as it provided the best modelling according to the sensitivity analysis performed to the results of the parameters included in the Pritchard and Hogg (2003) transport equation (see Mancini et al., 2020).

Table 2: Main parameters in the Pritchard and Hogg (2003) transport equation

Pritchard and Hogg (2003) equation		
m_e	=	0.01 m/s
$\tau_{b,cr}$	=	0 N/m^2
R	=	1.5
λ	=	H_{rms} (i.e., root-means-square wave height) at WG3
τ_{ref}	=	$\rho c_{f,ref} u_{ref} \lvert u_{ref} \rvert$, where $c_{f,ref} = gn^2/\lambda^{1/3}$ and $u_{ref} = \sqrt{g\lambda}$

Comparison with Alsina et al. (2016) For the hydrodynamics modelling of XBNH-WAST and XBNH-IWST, the reader is referred to Ruffini et al. (2020) and Mancini et al. (2020), respectively. Here, only results for the sediment transport and in turn, for the morphodynamics modelling of the two approaches considered in this study are shown.

Fig. 2 (a, c) shows the final bed changes, $\Delta z_{b_f} = z_b(t = t_f, x) - z_b(0, x)$ (with t_f being the time at the end of SEG2), for BE1_2 and BE4_2, respectively. For both XBNH-WAST and XBNH-IWST, numerical results show a better performance for BE1_2 than BE4_2 in both the surf and swash zone. For BE1_2, unlike XBNH-WAST, the newly included XBNH-IWST approach is able to predict the deposition in the upper swash zone, which is located slightly offshore than the observed one due to the underestimation of the wave run-up. Instead, for both wave conditions, either XBNH-WAST or XBNH-IWST are not able to accurately reproduce the formation of the breaker bar in the surf zone.
The net sediment transport rate, $\bar{q}_{sed}$, over SEG1 and SEG2 is shown in Figs. 2 (b, d) for BE1_2 and BE4_2, respectively. This was computed using a sediment balance, which was numerically integrated over the x-domain between the start of SEG1 and the end of SEG2:

$$\bar{q}_{sed}(x = x_i) = \bar{q}_{sed}(x = x_{i-1}) - (1 - n_p)\frac{\Delta z_{b_{SEG1-2}} \Delta x}{\Delta t_{SEG1-2}}, \tag{17}$$

where q_{sed} is the instantaneous sediment transport and the bar refers to the averaging over the duration of the two segments, Δt_{SEG1-2}; the subscript i refers to the $i-$th point along the $x-$domain for both the numerical mesh and the experimental domain, where z_b is available. Thus, $i = 1, ...N$, with i =1 at the onshore boundary of the domain (i.e., landward of the maximum run-up limit), where $q_{sed} = 0$ is assumed, and $i = N$ at the offshore start of the beach. $\Delta z_{b_{SEG1-2}}$ is the difference between z_b at the end of SEG2 and at the start of SEG1. Fig. 2 (b) highlights that XBNH-IWST is able to simulate the magnitude of the onshore-directed $\bar{q}_{sed}$ in the upper swash zone and the offshore-directed one in the lower swash region and surf zone up to the crest of the bar, located at $x = 65$ m. On the other hand, XBNH-WAST underestimates $\bar{q}_{sed}$ in the upper swash zone. Similarly, Fig. 2 (d) reveals that XBNH-IWST better captures the sign of $\bar{q}_{sed}$ in the upper swash zone than XBNH-WAST, but the magnitude is underestimated for both approaches. A more prominent bar was observed in BE4_2 than BE1_2, which both XBNH-WAST and XBNH-IWST cannot reproduce. Therefore, the exchange of sediment between the swash and surf zones is not well simulated, resulting in a deterioration in the overall modelling of $\bar{q}_{sed}$. Note that for BE4_2 the observed $\bar{q}_{sed}$ goes to zero at the offshore boundary, which is not shown in Fig. 2 (d). However, the positive and quasi-uniform value of the observed $\bar{q}_{sed}$ in the shoaling zone is most likely affected by measurement effects due to the mechanical wheel profiler used to measure the bed level. This instrument has a wheel that is too large to detect individual ripples. Therefore, the change in the bed level is below the sensitivity of the instrument.

Differences in the prediction of Δz_{b_f} and $\bar{q}_{sed}$ between XBNH-WAST and XBNH-IWST are due to a different reproduction of the time-histories of C, and in turn, of huC, which are illustrated in Fig. 3 (b, e and c, f, respectively) for BE1_2 and BE4_2. XBNH-ISWT is able to better describe the sediment suspension observed after the first bore generated by swash-swash interactions within the group and C close to flow reversal, from a qualitative point of view. For XBNH-WAST, unlike the observations, the predicted C

significantly decreases close to flow reversal (i.e., when u = 0 m/s). This is also reflected by the computed huC in 3 (f).

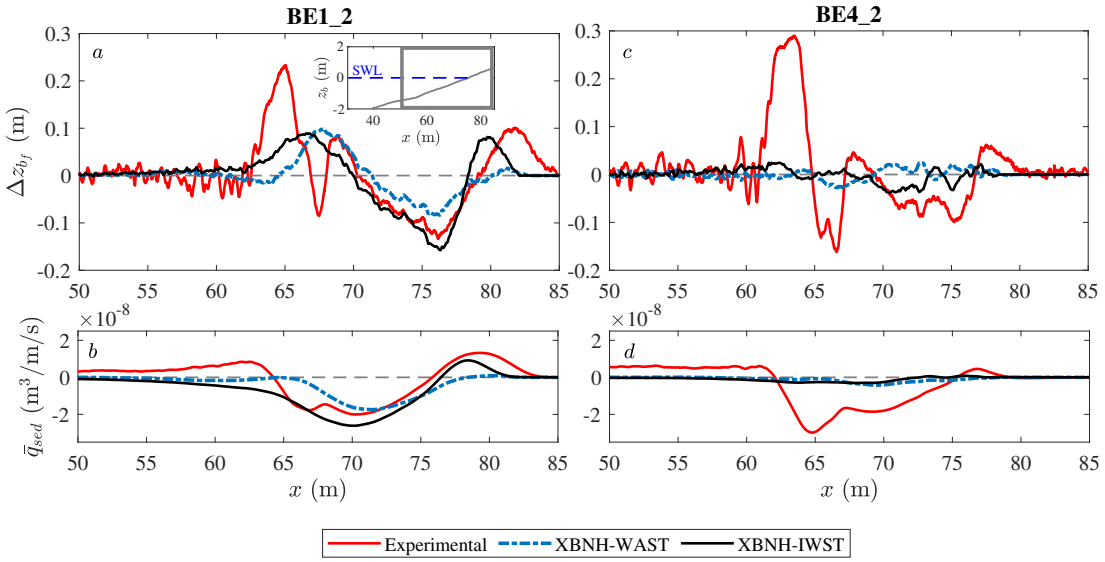

Figure 2: Comparison between XBNH-IWST and XBNH-WAST; results for Δz_{b_f} (a, c) and $\bar{q}_{sed}$ (c,d) for BE1_2 and BE4_2, respectively; reference line: grey-dashed line; the subplot in a indicates the region across the domain of the results shown in the main plots

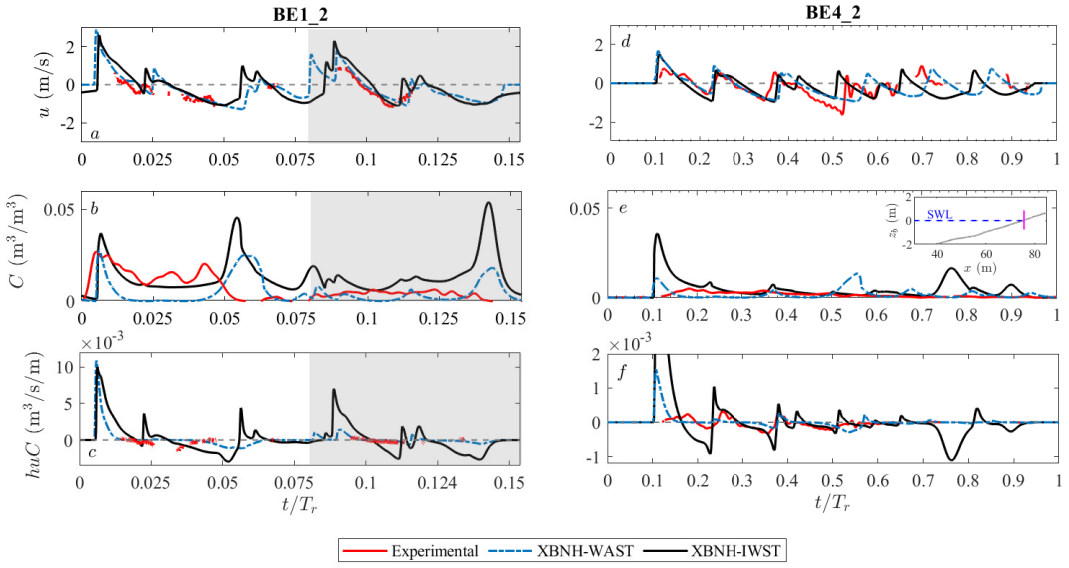

Figure 3: Comparison between XBNH-IWST and XBNH-WAST; time series of u (a,d) and C (b,e) and huC (c,f) at x = 75.81 m for BE1_2 and BE4_2, respectively; reference line: grey-dashed line; the shaded area distinguishes the two wave groups in a, b and c; the subplot in e indicates the selected x–location in the domain. Note that the maximum value of the modelled huC for XBNH-IWST in f is 0.0075 m^3/s/m (at $t/T_r \sim$ 0.11)

DISCUSSION

Numerical simulations of the laboratory experiments of Alsina et al. (2016) revealed that the newly implemented wave-resolving XBNH-IWST approach better describes the intra-swash C than XBNH-WAST. Consequently, XBNH-IWST better simulates the deposition in the upper swash zone and the erosion in the lower swash region. In fact, Δz_{b_f} predicted with XBNH-WAST diverges from observations, especially in the upper swash zone. This might be explained by the behaviour of the sediment transport model in XBNH-IWST near flow reversal (i.e., $u = 0$ m/s), when sediment particles are allowed to settle. Note that the upper swash bar predicted with XBNH-IWST is located slightly offshore of the observed one. This is due to the underestimation of the wave run up with XBNH, which is found to be consistent with previous studies (see also Van Rooijen et al., 2012). The better performance of XBNH-IWST than XBNH-WAST for Δz_{b_f} is quantitatively confirmed by the corresponding nRMSE reported in Table 3. The higher accuracy of XBNH-IWST than XBNH-WAST is by 20% for BE1_2, while the accuracy is comparable for BE4_2.

Table 3: nRMSE for Δz_{b_f} for BE1_2 and BE4_2, respectively; comparison between XBNH-IWST and XBNH-WAST

	BE1_2		BE4_2	
	XBNH-IWST	**XBNH-WAST**	**XBNH-IWST**	**XBNH-WAST**
nRMSE	0.0464	0.0575	0.0712	0.0750

The corresponding nRMSE and ρ_{mr} for C are presented in Table 4. The accuracy of XBNH-IWST in the prediction of C in terms of nRMSE and ρ_{mr} is similar to that of XBNH-WAST. For both approaches the values of ρ_{mr} reflect a poor correlation between the predicted and observed C.

Table 4: nRMSE and ρ_{mr} for C for BE1_2 and BE4_2, respectively; comparison between XBNH-IWST and XBNH-WAST

	BE1_2		BE4_2	
	XBNH-IWST	**XBNH-WAST**	**XBNH-IWST**	**XBNH-WAST**
nRMSE	1.3333	1.2906	5.9385	2.3647
ρ_{mr}	0.0785	-0.1005	0.2696	0.1405

For both wave conditions, some limitations are visible for the two modelling approaches in the shoaling region and the surf zone up to the bar crest, where the experimental onshore-directed $\bar{q}_{sed}$ is not predicted by both approaches. When the experimental $\bar{q}_{sed}$ changes in sign, the modelled ones continue being negative for both wave conditions. Consequently, the exchange of sediments between the swash zone and the surf zones, and in turn, the breaker bar development process are not accurately reproduced.

XBNH misses an explicit representation of physical processes, such as the wave breaking-generated turbulence and phasing-effects of the velocity in the bottom boundary layer. In their study Zhang and Liu (2008) found out an earlier flow reversal near the bottom with respect to the rest of the water column in the swash zone. Moreover, despite XBNH accounting for a depth-averaged net return current, the vertical structure of the sediment concentration and flow in a suitable formulation for the models at hand could play a key role in the simulation of the intra-wave sediment dynamics in both the swash zone and surf zones (see also Mancini et al., 2020).

CONCLUSION

In this study an analysis of the performance of different sediment transport formulations in XBNH was conducted. In particular, the XBNH-IWST approach, considering the wave-resolving Pritchard and Hogg (2003) transport equation and the Meyer-Peter and Müller (1948) expression, was newly implemented in XBNH. The performance of XBNH-IWST was compared with the existing XBNH-WAST approach, originally developed and validated for the wave-averaged version of XBeach. The two approaches were tested against the laboratory experiments of Alsina et al. (2016), involving wave trains and where swash-swash interactions were present. Additionally, in Mancini et al. (2020) XBNH-IWST was verified against the semi-analytical solution of Zhu and Dodd (2015) and tested with the laboratory experiments of Young

et al. (2010) involving non-interacting solitary waves over a 1:15 sloped beach, showing a good performance in the simulation of the intra-wave sediment transport and in turn, of the beach morphodynamics.

Numerical results showed that XBNH-IWST better describes the bed changes in the upper and lower swash regions with respect to XBNH-WAST, both quantitatively and qualitatively. This reveals that a wave-resolving approach for the sediment transport modelling is necessary for simulating the swash morphodynamics with XBNH. However, the accuracy in the prediction of the time-history of C is similar for XBNH-IWST and XBNH-WAST, resulting in a poor correlation between the modelled and experimental C. Also, both approaches are not able to accurately capture the processes of the bar formation in the surf zone. Future work will be carried out to explicitly include further physical processes that the model lacks for improving the prediction of the mutual feedback between the swash zone and the surf zone, and to address the issue of erosion and recovery cycles in storms clusters (Besio et al., 2017).

ACKNOWLEDGEMENTS

This work is part of the doctoral thesis of Miss Giulia Mancini. The experimental part of the bichromatic wave groups was funded by European Community's Seventh Framework Programme through the grant of the Integrating Activity HYDRALAB IV within the Transnational Access Activities; contract no. 261520.

References

Alsina, J.M., Cáceres, I., Brocchini, M., Baldock, T.E., 2012. An experimental study on sediment transport and bed evolution under different swash zone morphological conditions. *Coastal Engineering* 68, 31–43.

Alsina, J.M., Padilla, E.M., Cáceres, I., 2016. Sediment transport and beach profile evolution induced by bi-chromatic wave groups with different group periods. *Coastal Engineering* 114, 325–340.

Bai, Y., Yamazaki, Y., Fai Cheung, K., 2018. Convergence of multilayer nonhydrostatic models in relation to Boussinesq-type equations. *Journal of Waterway, Port, Coastal, and Ocean Engineering* 144(2), 06018001.

Besio, G., Briganti, R., Romano, A., Mentaschi, L., De Girolamo, P., 2017. Time-clustering of wave storms in the mediterranean sea. *Natural Hazards and Earth System Sciences* 17.

Briganti, R., Dodd, N., Incelli, G., Kikkert, G., 2018. Numerical modelling of the flow and bed evolution of a single bore-driven swash event on a coarse sand beach. *Coastal Engineering* 142, 62–76.

Briganti, R., Torres-Freyermuth, A., Baldock, T.E., Brocchini, M., Dodd, N., Hsu, T.J., Jiang, Z., Kim, Y., Pintado-Patiño, J.C., Postacchini, M., 2016. Advances in numerical modelling of swash zone dynamics. *Coastal Engineering* 115, 26–41.

Chardón-Maldonado, P., Pintado-Patiño, J.C., Puleo, J.A., 2016. Advances in swash-zone research: Small-scale hydrodynamic and sediment transport processes. *Coastal Engineering* 115, 8–25.

Deltares, 2015. XBeach documentation, <https://xbeach.readthedocs.io> .

Incelli, G., Dodd, N., Blenkinsopp, C.E., Zhu, F., Briganti, R., 2016. Morphodynamical modelling of field-scale swash events. *Coastal Engineering* 115, 42–57.

Jacobsen, N.G., Fredsoe, J., Jensen, J.H., 2014. Formation and development of a breaker bar under regular waves. part 1: Model description and hydrodynamics. *Coastal Engineering* 88, 182–193.

Kim, D.H., Sanchez-Arcilla, A., Caceres, I., 2017. Depth-integrated modelling on onshore and offshore sandbar migration: Revision of fall velocity. *Ocean Modelling* 110, 21 – 31.

Kim, Y., Mieras, R.S., Cheng, Z., Anderson, D., Hsu, T.J., Puleo, J.A., Cox, D., 2019. A numerical study of sheet flow driven by velocity and acceleration skewed near-breaking waves on a sandbar using sedwavefoam. *Coastal Engineering* 152, 103526.

Larsen, B.E., van der Zanden, J., Ruessink, G., Fuhrman, D.R., et al., 2020. Stabilized rans simulation of surf zone kinematics and boundary layer processes beneath large-scale plunging waves over a breaker bar. *Ocean Modelling* 155, 101705.

Li, J., Qi, M., Fuhrman, D.R., 2019. Numerical modeling of flow and morphology induced by a solitary wave on a sloping beach. *Applied Ocean Research* 82.

Ma, G., Shi, F., Kirby, J.T., 2012. Shock-capturing non-hydrostatic model for fully dispersive surface wave processes. *Ocean Modelling* 43, 22–35.

Mancini, G., Briganti, R., McCall, R., Dodd, N., Zhu, F., 2020. Numerical modelling of intra-wave sediment transport on sandy beaches using a non-hydrostatic, wave-resolving model. *Ocean Dynamics* , 1–20.

McCall, R., Masselink, G., Poate, T., Roelvink, J., Almeida, L., 2015. Modelling the morphodynamics of gravel beaches during storms with XBeach-G. *Coastal Engineering* 103, 52–66.

Meyer-Peter, E., Müller, R., 1948. Formulas for bed-load transport, *in: IAHSR 2nd meeting, Stockholm, appendix 2*, IAHR.

O'Donoghue, T., Kikkert, G.A., Pokrajac, D., Dodd, N., Briganti, R., 2016. Intra-swash hydrodynamics and sediment flux for dambreak swash on coarse-grained beaches. *Coastal Engineering* 112, 113–130.

Postacchini, M., Brocchini, M., Mancinelli, A., Landon, M., 2012. A multi-purpose, intra-wave, shallow water hydro-morphodynamic solver. *Advances in Water Resources* 38, 13–26.

Pritchard, D., Hogg, A.J., 2003. Suspended sediment transport under seiches in circular and elliptical basins. *Coastal Engineering* 49(1-2), 43–70.

Ruffini, G., Briganti, R., Alsina, J., Brocchini, M., Dodd, N., McCall, R., 2020. Numerical modelling of flow and bed evolution of bichromatic wave groups on an intermediate beach using non-hydrostatic XBeach. *Journal of Waterway, Port, Coastal, and Ocean Engineering* 146(1).

Smagorinsky, J., 1963. General circulation experiments with the primitive equations: I. the basic experiment. *Monthly weather review* 91(3), 99–164.

Smit, P., Stelling, G., Roelvink, D., van Thiel de Vries, J., McCall, R., van Dongeren, A., Zwinkels, C., Jacobs, R., 2010. XBeach: Non-hydrostatic model. *Delft University of Technology and Deltares* .

Smit, P., Zijlema, M., Stelling, G., 2013. Depth-induced wave breaking in a non-hydrostatic, near-shore wave model. *Coastal Engineering* 76, 1–16.

Soulsby, R., 1997. Dynamics of marine sands: a manual for practical applications. Thomas Telford.

Van Rijn, L., Ruessink, G., Grasmeijer, B., van der Werf, J., Ribberink, J., 2007. Wave-related transport and nearshore morphology, *in: Coastal Sediments' 07*, pp. 1–14.

Van Rijn, L.C., 2007. Unified view of sediment transport by currents and waves. i: Initiation of motion, bed roughness, and bed-load transport. *Journal of Hydraulic Engineering* 133(6), 649–667.

Van Rooijen, A., Reniers, A., Van Thiel de Vries, J., Blenkinsopp, C., McCall, R., 2012. Modeling swash zone sediment transport at truc vert beach, *in: ICCE 2012: Proceedings of the 33rd International Conference on Coastal Engineering, Santander, Spain, 1-6 July 2012*, Coastal Engineering Research Council.

Van Thiel de Vries, J., 2008. Dune erosion during storm surges. Ph.D. thesis. Technical University of Delft.

Xiao, H., Young, Y.L., Prévost, J.H., 2010. Hydro-and morpho-dynamic modeling of breaking solitary waves over a fine sand beach. part ii: Numerical simulation. *Marine Geology* 269(3-4), 119–131.

Young, Y.L., Xiao, H., Maddux, T., 2010. Hydro-and morpho-dynamic modeling of breaking solitary waves over a fine sand beach. part i: Experimental study. *Marine Geology* 269(3-4), 107–118.

Zhang, Q., Liu, P.L.F., 2008. A numerical study of swash flows generated by bores. *Coastal Engineering* 55(12), 1113–1134.

Zhu, F., Dodd, N., 2015. The morphodynamics of a swash event on an erodible beach. *Journal of Fluid Mechanics* 762, 110–140.

Zijlema, M., Stelling, G., Smit, P., 2011. Swash: An operational public domain code for simulating wave fields and rapidly varied flows in coastal waters. *Coastal Engineering* 58(10), 992–1012.